Article

Evidence of a $J/\psi\Lambda$ structure and observation of excited Ξ^- states in the $\Xi_b^- \to J/\psi\Lambda K^-$ decay

LHCb Collaboration [1]

A R T I C L E   I N F O

A B S T R A C T

First evidence of a structure in the $J/\psi\Lambda$ invariant mass distribution is obtained from an amplitude analysis of $\Xi_b^- \to J/\psi\Lambda K^-$ decays. The observed structure is consistent with being due to a charmonium pentaquark with strangeness with a significance of 3.1σ including systematic uncertainties and look-elsewhere effect. Its mass and width are determined to be $4458.8 \pm 2.9^{+4.7}_{-1.1}$ MeV and $17.3 \pm 6.5^{+8.0}_{-5.7}$ MeV, respectively, where the quoted uncertainties are statistical and systematic. The structure is also consistent with being due to two resonances. In addition, the narrow excited Ξ^- states, $\Xi(1690)^-$ and $\Xi(1820)^-$, are seen for the first time in a Ξ_b^- decay, and their masses and widths are measured with improved precision. The analysis is performed using pp collision data corresponding to a total integrated luminosity of 9 fb^{-1}, collected with the LHCb experiment at centre-of-mass energies of 7, 8 and 13 TeV.

1. Introduction

The existence of pentaquark states, comprising four quarks and an antiquark, has been anticipated since the establishment of the quark model [1,2]. The first observation of pentaquark states has been reported by the LHCb experiment [3]. In the analysis of $\Lambda_b^0 \to J/\psi(\to \mu^+\mu^-)pK^-$ decays, a narrow structure in the $J/\psi p$ mass spectrum indicated a possible pentaquark contribution [3,4] (Charge conjugation is implied and natural units with $\hbar = c = 1$ are used throughout this article). An amplitude analysis showed that the data could be best described by the presence of two pentaquark states, the $P_c(4380)^+$ and $P_c(4450)^+$. With the inclusion of additional data and an improved selection strategy, it was found that the $P_c(4450)^+$ could be resolved into two narrow states, the $P_c(4440)^+$ and $P_c(4457)^+$. In addition, a new narrow state, the $P_c(4312)^+$ was discovered [5]. The $[uudc\bar{c}]$ valence quark content is attributed to these pentaquark states. Their strange counterparts, denoted P_{cs}^0, with $[udsc\bar{c}]$ valence quark content, are predicted in Refs. [6–11] and it has been suggested to search for them in $\Xi_b^- \to J/\psi\Lambda K^-$ decays [8,12].

The $\Xi_b^- \to J/\psi\Lambda K^-$ decay also provides the opportunity to study excited Ξ^- resonances (denoted collectively as Ξ^{*-}) in a mass range of [1.61, 2.70] GeV, where only a small number of Ξ^{*-} states have been observed, with a typical uncertainty of more than 5 MeV on

their masses and widths [13]. Five Ξ^{*-} states have been established experimentally, the $\Xi(1530)^-$, $\Xi(1690)^-$, $\Xi(1820)^-$, $\Xi(1950)^-$ and $\Xi(2030)^-$. Recently, several results on the $\Xi(1690)^-$ and $\Xi(1820)^-$ states have been reported by the BESIII Collaboration [14,15]. For the neutral partners, the Belle Collaboration observed a $\Xi(1620)^0$ resonance and found evidence for a $\Xi(1690)^0$ state in $\Xi_c^+ \to \Xi^-\pi^+\pi^+$ decays [16]. More studies of excited Ξ states will improve our understanding of the Ξ spectrum and of the structure of baryon resonances.

In this article, an amplitude analysis of the $\Xi_b^- \to J/\psi\Lambda K^-$ decay is performed using proton-proton (pp) collision data collected at centre-of-mass energies of $\sqrt{s} = 7$ and 8 TeV, corresponding to an integrated luminosity of 3 fb^{-1} (Run 1) and at $\sqrt{s} = 13$ TeV, corresponding to 6 fb^{-1} (Run 2). The LHCb Collaboration first observed the decay $\Xi_b^- \to J/\psi\Lambda K^-$ using Run 1 data and measured the production rate of Ξ_b^- with $\Xi_b^- \to J/\psi\Lambda K^-$ decays relative to that of $\Lambda_b^0 \to J/\psi\Lambda$ decays [17].

2. Detector and data set

The LHCb detector [18,19] is a single-arm forward spectrometer covering the pseudorapidity range $2 < \eta < 5$, designed for the study of particles containing b or c quarks. The detector includes a silicon-strip vertex detector surrounding the proton-proton interaction region, tracking stations on either side of a dipole magnet, ring-imaging Cherenkov (RICH) detectors, calorimeters and

---

muon chambers. Simulation is required to evaluate the detector acceptance in the full phase space of $\Xi_b^- \to J/\psi\Lambda K^-$ decays and the efficiency of signal selection. In the simulation, pp collisions are generated using PYTHIA [20] with a specific LHCb configuration [21]. Decays of unstable particles are described by EVTGEN [22], in which final-state radiation is generated using PHOTOS [23,24]. The interaction of the generated particles with the detector, and its response, are implemented using the GEANT4 toolkit [25,26] as described in Ref. [27]. The production kinematics of Ξ_b^- baryons in the simulation is corrected based on the two-dimensional distribution of the momentum component transverse to the beam direction (p_T) and rapidity (y) obtained using a sample of $\Lambda_b^0 \to J/\psi\Lambda$ decays selected from data.

The $\Xi_b^- \to J/\psi(\to \mu^+\mu^-)\Lambda(\to p\pi^-)K^-$ signal candidates are first required to pass an online event selection performed by a trigger [28], consisting of a hardware stage that is based on information from the calorimeters and the muon system, followed by two software stages that perform a partial event reconstruction. At the hardware stage, events are required to have a muon with a high momentum component transverse to the beam direction (p_T) or a hadron, photon or electron with a high transverse energy. In the first software stage, the event is required to have either two well-identified oppositely charged muons with large invariant mass, or at least one muon with $p_T > 1$ GeV and a large impact-parameter significance with respect to any primary pp collision vertex (PV). In the second stage, events containing a $\mu^+\mu^-$ pair with invariant mass consistent with the known J/ψ mass [13], and with a vertex significantly displaced from any PV, are selected. Candidate $\Lambda \to p\pi^-$ decays are reconstructed in two different categories: long involving Λ baryons with a flight distance short enough for the proton and pion to have the decay vertex reconstructed in the vertex detector; and downstream containing Λ baryons decaying later such that the track segments of the proton and pion cannot be formed in the vertex detector and are reconstructed only in the tracking stations. The candidates in the long category have better mass, momentum and decay vertex resolution than those in the downstream category. A Ξ_b^- candidate is then reconstructed by combining the J/ψ, Λ and a well identified K^- candidate, which are required to form a good-quality vertex.

3. Candidate selection

Candidates are required to pass a set of selection criteria and are then further filtered using a multivariate classifier based on a gradient boosted decision tree (BDTG) [29–31]. The selection criteria are almost identical to those used in the previous analysis [17], except those on the p_T of the Λ decay products and on the χ_{IP}^2 of the kaon candidate which are relaxed. The χ_{IP}^2 is defined as the difference in the vertex-fit χ^2 of a given PV reconstructed with and without the track considered. In total, 15 variables are combined to train the BDTG classifier. The requirement of the BDTG response is selected to maximise the signal significance, separately for four categories (long and downstream Λ candidates in Run 1 and 2). In the selected sample, less than 0.5% of the events contain more than one Ξ_b^- candidate, which are all retained.

A kinematic fit [32] is applied to the Ξ_b^- decay to improve the mass resolution where the J/ψ and Λ candidate masses are constrained to their known values [13], and the Ξ_b^- candidate is constrained to originate from a primary vertex. The resulting $J/\psi\Lambda K^-$ invariant mass spectra for the four categories are shown in Fig. 1. The total signal yield is 1750 ± 50, determined by an unbinned extended maximum-likelihood fit to the $J/\psi\Lambda K^-$ invariant mass spectra for each of the four categories. The signal is described by a Hypatia function [33], while combinatorial background is modelled by an exponential function. Partially

reconstructed $\Xi_b^- \to J/\psi\Sigma^0(\to \Lambda\gamma)K^-$ decays form a specific background at masses below the known Ξ_b^- mass. The shape of this background is determined using a non-parametric model from simulation. Its yield varies freely in the fit. Weights [34] are assigned to the candidates to statistically subtract background contributions by weighting each candidate depending on their invariant $J/\psi\Lambda K^-$ mass. A kinematic fit is performed to improve the momentum resolution of final-state particles by further constraining the Ξ_b^- candidate mass to its known value [13]. The resulting Dalitz plot for candidates within ± 15 MeV of the Ξ_b^- peak position is shown in Fig. 2. As expected, significant $\Xi^{*-} \to \Lambda K^-$ contributions, in particular from the $\Xi(1690)^-$ and $\Xi(1820)^-$ resonances, are observed. The $J/\psi\Lambda$ mass spectrum will be further explored in this article.

4. Amplitude analysis

An amplitude analysis is carried out to measure the properties of the $\Xi(1690)^-$ and $\Xi(1820)^-$ resonances, and to examine a possible contribution from any P_{cs}^0 pentaquark states decaying into $J/\psi\Lambda$. The amplitude fits minimise an unbinned negative log-likelihood, $\mathcal{L}$, constructed in a six-dimensional phase space of the data [3]. The six dimensions correspond to the ΛK^- mass and five angular observables $\theta_{\Xi_b^-}$, θ_{Ξ^-}, $\theta_{J/\psi}$, ϕ_Λ, ϕ_μ, where θ and ϕ denote the polar and azimuthal angles, respectively. The probability distribution function only comprises the contribution from signal Ξ_b^- decays, since the background is subtracted using the sPlot technique [34,35], as discussed in detail in Ref. [3]. The efficiency on the six-dimensional phase space is folded into the signal probability density function. The amplitude analysis follows a similar strategy to that of $\Lambda_b^0 \to J/\psi pK^-$ decays in Ref. [3], with the Λ_b^0 baryon and proton in the Λ_b^0 decay replaced by the Ξ_b^- and Λ baryons, respectively. However, a cross-check with the Dalitz-plot decomposition method proposed in Ref. [36] indicates that the method used in Ref. [3] has to be modified in two aspects to properly align the helicity state of the spin–half Λ baryon in the Ξ^{*-} and P_{cs}^0 decay chains [37]. First, in the $\Xi^{*-} \to \Lambda K^-$ decay, the Λ particle is used to define the two decay angles of the Ξ^{*-} system. The definition of the remaining angles is the same as in Ref. [3]. Secondly, the Euler rotation in the $\Xi^{*-} \to \Lambda K^-$ decay aligns the spin axis along the Λ momentum, while the rotation in the $P_{cs}^0 \to J/\psi\Lambda$ frame aligns the spin axis in the direction opposite to the Λ momentum. An additional rotation to align the z-axis between the P_{cs}^0 and Ξ^{*-} chains generates a term $(-1)^{J_\Lambda - \lambda_\Lambda^{P_{cs}}}$ in the amplitude of the P_{cs}^0 chain, where J_Λ and $\lambda_\Lambda^{P_{cs}}$ are the spin and the helicity of the Λ particle in the P_{cs}^0 rest frame, respectively. This term is the particle-two convention factor [38].

Table 1 lists the possible contributions from well established Ξ^{*-} states according to the PDG [13]. The states constitute a default description of the ΛK^- invariant mass spectrum, which is also assumed to include a nonresonant (NR) contribution. As the spin-parities of these resonances are unknown except for that of the $\Xi(1820)^-$ baryon, combinations of different J^P of these states are examined in the amplitude fit. Due to limited sample size, each Ξ^{*-} resonance is described by 3 or 4 independent LS couplings, where L stands for the decay orbital angular momentum, and S is the sum of spins of the decay products. Couplings corresponding to higher L are expected to be suppressed by the angular momentum barrier, so the contributions are chosen in increasing order of L. For all Ξ^{*-} resonances, relativistic Breit-Wigner functions [3] are used to model their line shape and phase variation as a function of the invariant mass of the ΛK^- system, $m_{\Lambda K^-}$. The masses and widths of the $\Xi(1690)^-$ and $\Xi(1820)^-$ resonances are free fit
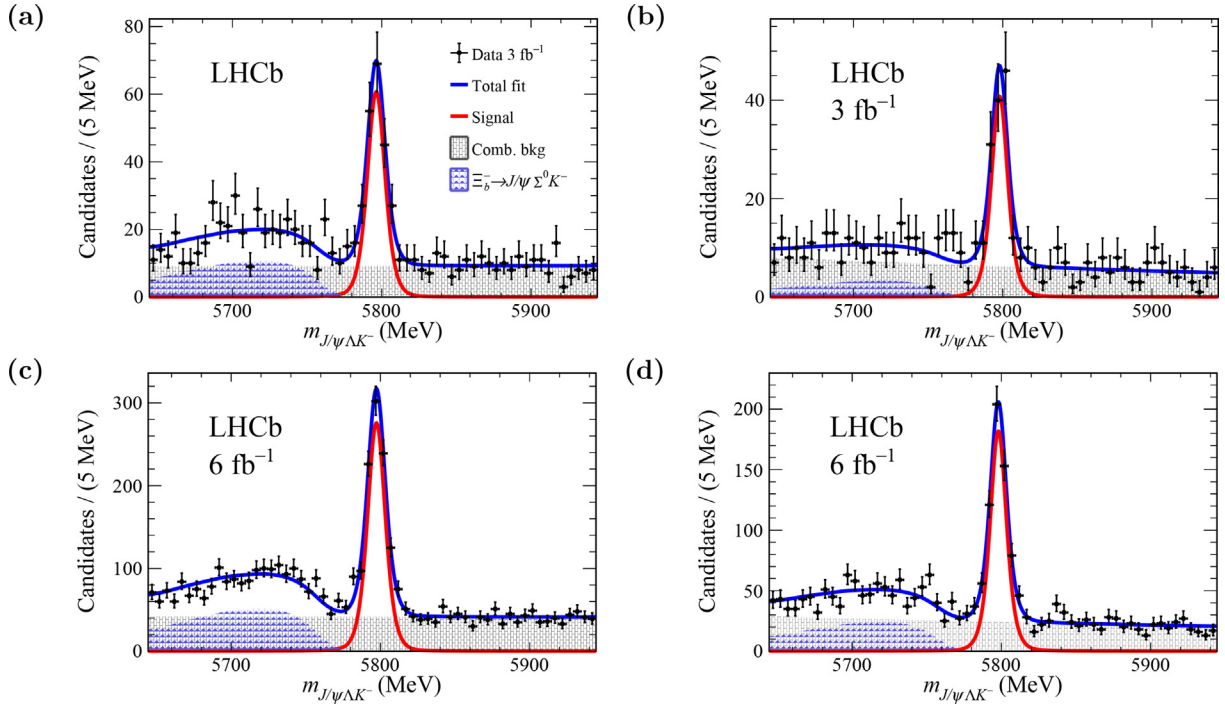
Fig. 1. Invariant mass distributions of selected $\Xi_b^- \to J/\psi \Lambda K^-$ candidates in the (a) Run 1 downstream, (b) Run 1 long, (c) Run 2 downstream, and (d) Run 2 long samples. The data are overlaid by the result of the fit described in the text.
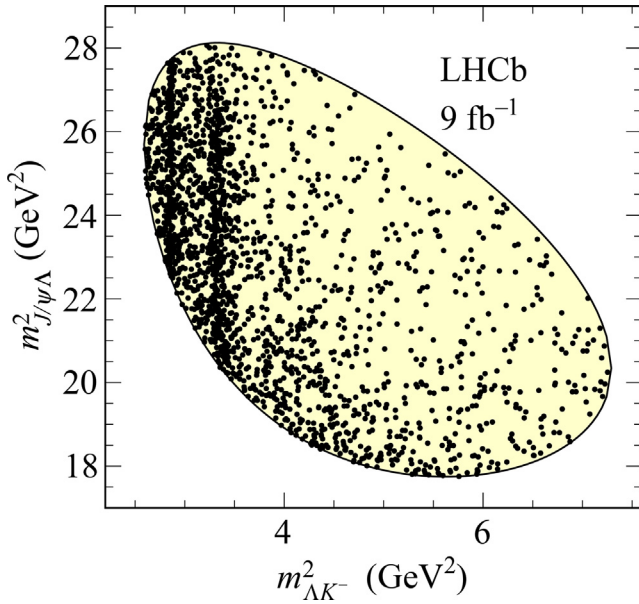

Fig. 2. Dalitz plot for all candidates within ± 15 MeV of the known Ξ_b^- mass. The yellow area shows the kinematically allowed region.

Table 1
The components in the amplitude fit used to describe the ΛK^- system. The J^P, masses (M_0) and widths (Γ_0) of the Ξ^- states are taken from the PDG [13]. The numbers of LS couplings used in the default fit are listed, together with the total number of the LS couplings associated to the ΛK^- component, given in parentheses. The $\Xi(1820)^-$ coupling of lowest LS is set to (1,0) for reference. Multiple J^P assignments are considered for states where this assignment has not been previously established. A nonresonant S-wave ΛK^- contribution, labelled as NR, is also considered in the fit model.

State	M_0 (MeV)	Γ_0 (MeV)	LS couplings	J^P examined
$\Xi(1690)^-$	1690 ± 10	< 30	4 (6)	$(1/2, 3/2)^{\pm}$
$\Xi(1820)^-$	1823 ± 5	24^{+15}_{-10}	3 (6)	$3/2^-$
$\Xi(1950)^-$	1950 ± 15	60 ± 20	3 (6)	$(1/2, 3/2, 5/2)^{\pm}$
$\Xi(2030)^-$	2025 ± 5	20^{+15}_{-5}	3 (6)	$5/2^{\pm}$
NR ΛK^-	-	-	4 (4)	$1/2^-$

parameters, while those of other Ξ^{*-} resonances are constrained by their known uncertainties [13]. The contribution of the NR S-wave component to the $m_{\Lambda K^-}$ spectrum is described with a function that is inversely proportional to $m^2_{\Lambda K^-}$ [39]. Alternative descriptions of the NR component are considered to estimate systematic uncertainties on the model. The ΛK^- and $J/\psi \Lambda$ mass spectra are shown in Fig. 3 with the projections of amplitude fit overlaid.

After the determination of the amplitude model with ΛK^--only contributions, a P^0_{cs} state is added to the amplitude model, with spin hypotheses ranging from 1/2 to 5/2 and parity hypotheses of both -1 and $+1$. Only the smallest allowed L is considered due to the suppression of higher values of L. A $J/\psi \Lambda$ mass resolution of 2.6 MeV obtained from simulation is taken into account by smearing the P^0_{cs} Breit-Wigner amplitude accordingly. The fits show a significant improvement when adding the P^0_{cs} state. The largest improvement on $-2 \ln \mathcal{L}$ when adding a single P^0_{cs} contribution is found to be $\Delta 2 \ln \mathcal{L} = 43$, for an addition of 6 parameters. This fit, which includes the ΛK^- resonances in Table 1, a NR ΛK^- component and a single P^0_{cs} state each with their favoured J^P assignment is referred to below as the default fit. The improvement in $-2 \ln \mathcal{L}$ corresponds to a statistical significance of 4.3 standard deviations (σ). This is estimated using pseudoexperiments where the look-elsewhere effect is taken into account. The difference of the $-2 \ln \mathcal{L}$ obtained using fit models with and without the contribution of the P^0_{cs} state is used as the test statistic to evaluate the p-value of the null hypothesis, where several alternative Ξ^{*-} models are used to describe the contributions from the ΛK^- resonances. The p-value is estimated by fitting the distribution of the test
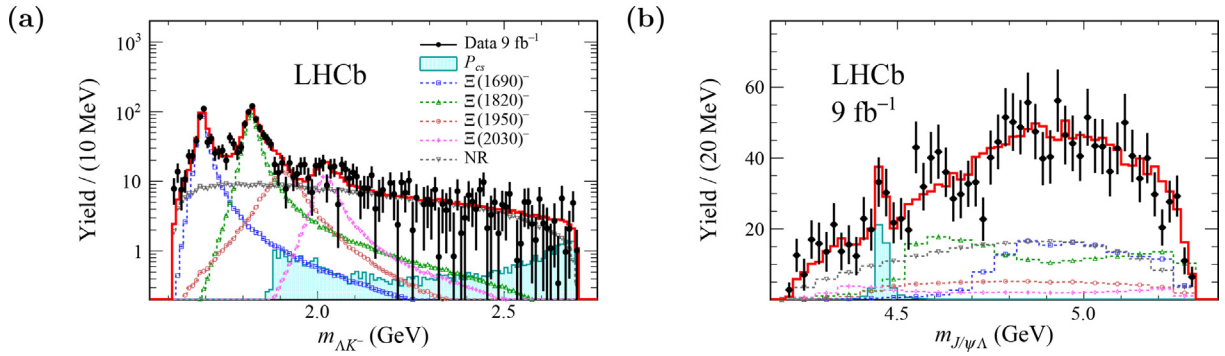
Fig. 3. The (a) $m_{\Lambda K^-}$ and (b) $m_{J/\psi\Lambda}$ distributions of selected candidates compared to the result of the fit with the P_{cs}^0 state.

statistic from 10,000 pseudoexperiments for the model based on the results from the fit to data fit, generated with the null hypothesis. To take into account the look-elsewhere effect for each pseudoexperiment, the global maximum of $2\ln\mathcal{L}$ is obtained by scanning the values of the mass and width of P_{cs}^0 state in the kinematically allowed region, instead of limiting their values to be consistent with that of the data fit. When including systematic uncertainties discussed below, the p-value is determined to be 0.2% by counting the fraction of pseudoexperiments with the $\Delta 2\ln\mathcal{L}$ value exceeding the smallest $\Delta 2\ln\mathcal{L}$ value from data. This p-value corresponds to the signal significance of 3.1σ with a two-sided Gaussian test for the P_{cs}^0 state, providing the first evidence for a charmonium pentaquark candidate with strangeness.

As shown in Fig. 3, the projections of the full amplitude fit onto the ΛK^- and $J/\psi\Lambda$ invariant mass spectra match the data distributions well. A test of the fit quality is performed by comparing the default fit of the Dalitz plot with the data distribution. The data is divided into 64 bins containing approximately the same number of decays. The χ^2 is calculated to be 77 for these bins, indicating a reasonably good description of the data. The P_{cs}^0 state is determined to have a mass of 4458.8 ± 2.9 (stat) MeV and a width of 17.3 ± 6.5 (stat) MeV, and hereafter is denoted as $P_{cs}(4459)^0$. Fig. 4 highlights the $P_{cs}(4459)^0$ contribution by comparing the fits to the $m_{J/\psi\Lambda}$ and $\cos\theta_{P_{cs}}$ distributions with and without the $P_{cs}(4459)^0$ state included, where $\theta_{P_{cs}}$ is the helicity angle of the $J/\psi\Lambda$ system, defined as the angle between the direction of the J/ψ particle and the opposite direction of the K^- particle in the $J/\psi\Lambda$ rest frame. The $P_{cs}(4459)^0$ state is more visible when the dominant contributions from Ξ^{*-} with low masses are suppressed by requiring $m_{\Lambda K^-} > 2.2$ GeV. As shown in Fig. 4b, a significant improvement of the fit quality is also found in the $\cos\theta_{P_{cs}}$ distribution when including the $P_{cs}(4459)^0$ state.

No evidence for any other P_{cs}^0 state is found in the considered mass range. This is also clear when examining the $m_{J/\psi\Lambda}$ projections in three intervals of $m_{\Lambda K^-}$, shown in Fig. 5. The measured mass, width and fit fraction (FF) of all components involved in the default fit are shown in Table 2. Systematic uncertainties on these results are discussed below.

The measured $P_{cs}(4459)^0$ mass is about 19 MeV below the $\Xi_c^0\bar{D}^{*0}$ threshold. In this region, Ref. [11] predicts two states with $J^P = 1/2^-$ and $3/2^-$ and a mass difference of 6 MeV. This is similar to the two $P_c(4440)^+$ and $P_c(4457)^+$ pentaquark states, which are just below the $\Sigma_c^+\bar{D}^{*0}$ threshold. Thus the hypothesis of a two-peak structure with the predicted J^P values is tested. The fit provides a good description of the data. The result is shown for the P_{cs}^0 enhanced region in Fig. 6. The masses and widths of the two states are 4454.9 ± 2.7 MeV and 7.5 ± 9.7 MeV, and 4467.8 ± 3.7 MeV and 5.2 ± 5.3 MeV, respectively, where the uncertainties are statistical only. The fit improves $2\ln\mathcal{L}$ by 4.8 units for 4 additional free parameters, compared to the fit using one Breit-Wigner function to model the structure. Therefore, the analysis of the current data sample cannot confirm or refute the two-peak hypothesis.

Systematic uncertainties are summarised in Table 3. Due to the limited number of candidates, J^P for the P_{cs}^0 state and for the $\Xi(1690)^-$, $\Xi(1950)^-$ and $\Xi(2030)^-$ states cannot be reliably determined. To estimate the systematic uncertainty related to the choice of J^P assignments, all possible J^P assignments for these states resulting in $-2\ln\mathcal{L}$ differences less than 9 units are compared to that from the default fit. The largest variation, with respect to the values in the default fit, is taken as an asymmetric systematic uncertainty. The uncertainty related to the fit model is estimated by: varying the hadron-size parameter in the Blatt-Weisskopf barrier factor [3] between 1.0 and 5.0 GeV^{-1}; modifying the orbital angular momenta L in Ξ_b^- decays that are used in the treatment
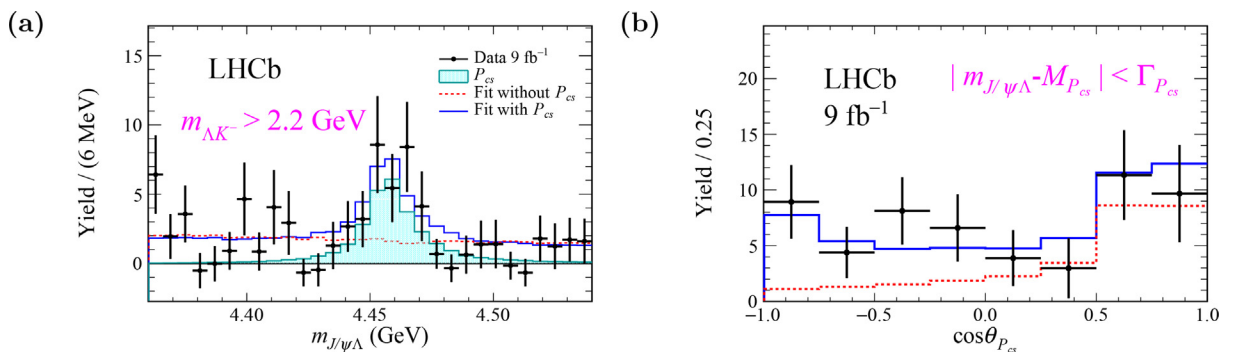
Fig. 4. (a) Projection of $m_{J/\psi\Lambda}$ in the range of $[4.36, 4.54]$ GeV with the $m_{\Lambda K^-} > 2.2$ GeV requirement. (b) Projection of $\cos\theta_{P_{cs}}$ for candidates having $m_{J/\psi\Lambda}$ within one natural width from the fitted P_{cs}^0 resonance mass. The red dashed lines show the result of the fit in Ξ^*-only hypothesis and the blue solid lines show the fit accounting for both Ξ^* and P_{cs}^0 states.
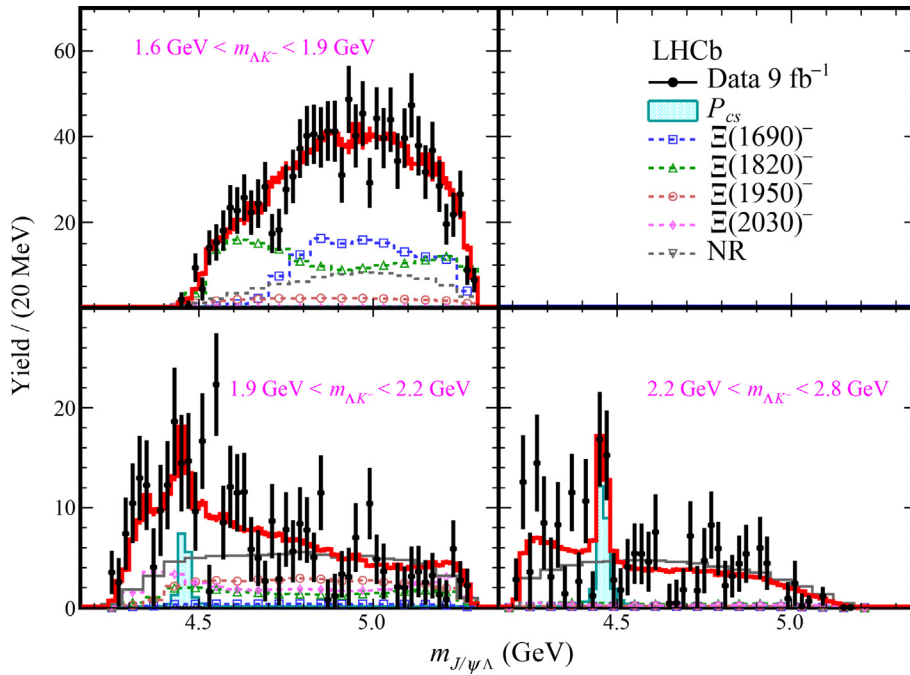
Fig. 5. Projections of $m_{J/\psi\Lambda}$ in intervals of (top left) $m_{\Lambda K^-} < 1.9$ GeV, (bottom left) $1.9 < m_{\Lambda K^-} < 2.2$ GeV, and (bottom right) $m_{\Lambda K^-} > 2.2$ GeV based on the default fit, superimposed with contributions from components listed in Table 1 and the P_{cs}^0 state.

Table 2

Mass (M_0), width (Γ_0) and fit fraction (FF) of the components involved in the default fit. The masses and widths of the P_{cs}^0, $\Xi(1690)^-$, and $\Xi(1820)^-$ resonances are free parameters, while those of the other Ξ^{*-} resonances are constrained by the known uncertainties [13]. The quoted uncertainties are statistical and systematic. When only one uncertainty is given, it is statistical.

State	M_0 (MeV)	Γ_0 (MeV)	FF (%)
$P_{cs}(4459)^0$	$4458.8 \pm 2.9^{+4.7}_{-1.1}$	$17.3 \pm 6.5^{+8.0}_{-5.7}$	$2.7^{+1.9+0.7}_{-0.6-1.3}$
$\Xi(1690)^-$	$1692.0 \pm 1.3^{+1.2}_{-0.4}$	$25.9 \pm 9.5^{+14.0}_{-13.5}$	$22.1^{+6.2+6.7}_{-2.6-8.9}$
$\Xi(1820)^-$	$1822.7 \pm 1.5^{+1.0}_{-0.6}$	$36.0 \pm 4.4^{+7.8}_{-8.2}$	$32.9^{+3.2+6.9}_{-6.2-4.1}$
$\Xi(1950)^-$	1910.6 ± 18.4	105.7 ± 23.2	$11.5^{+5.8+49.9}_{-3.5-9.4}$
$\Xi(2030)^-$	2022.8 ± 4.7	68.2 ± 8.5	$7.3^{+1.8+3.8}_{-1.8-4.1}$
NR	–	–	$35.8^{+4.6+10.3}_{-6.4-11.2}$
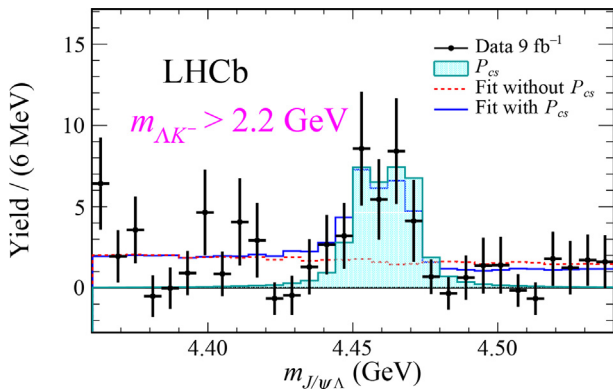
Fig. 6. Projection of $m_{J/\psi\Lambda}$ with a $m_{\Lambda K^-} > 2.2$ GeV requirement applied, overlaid by the fit using two resonances to model the peak region.

of the Ξ^{*-} resonances by one or two units; using all allowed couplings, instead of a limited number of L couplings, for Ξ^{*-} or $P_{cs}(4459)^0$ states; using alternative models to describe the nonres-

onant ΛK^- component, including an exponential function or a function inversely proportional to $m_{\Lambda K^-}^2 + m_{NR}^2$, where m_{NR} is a free parameter in the fit; considering the effects of Ξ_b^- polarisation, which are found to be consistent with zero in the analysis and neglected in the default fit; using an extended Ξ^{*-} model, which includes two more Ξ^{*-} states, in which the mass and width constraints on the Ξ^{*-} states are removed, and all allowed couplings for all Ξ^{*-} states are used. The largest value among all model variations is taken as systematic uncertainty for this source. The other systematic sources are estimated by: including the $\Lambda \rightarrow p\pi^-$ decay angles instead of taking the Λ baryon as a stable final-state particle; determining the sWeights by either splitting Ξ^{*-} helicity angles into bins or removing partially reconstructed physical background from the $\Xi_b^- \rightarrow J/\psi\Sigma^0(\rightarrow \Lambda\gamma)K^-$ decays in the [5644.5, 5764.5] MeV $J/\psi\Lambda K^-$ mass sideband; and varying the efficiency due to imperfect simulation. The mass resolution of the ΛK^- system is about 1–2 MeV, and has negligible effect on the fit due to the large widths of the Ξ^{*-} states. The significance for the $P_{cs}(4459)^0$ state is conservatively taken as the smallest significance found when combining different sources of systematic uncertainty together, and is equal to 3.1σ, as already reported, where the look-elsewhere effect has been taken into account. It corresponds to varying the hadron-size parameter in the extended Ξ^{*-} model with full couplings for the considered $P_{cs}(4459)^0$ state.

The negative systematic uncertainty for the $P_{cs}(4459)^0$ fit fraction, -1.3%, is obtained from an alternative value of J^P used for the $P_{cs}(4459)^0$ state. In such a fit, the significance of the $P_{cs}(4459)^0$ state is 4.1σ, even though the fit fraction is 1.4%. This is because the significance has contributions from two sources, the fit fraction and the interference fraction involving the $P_{cs}(4459)^0$ state. The interference fraction is about $+1.3\%$ in this alternative J^P fit, while it is almost 0 in the default fit. The systematic uncertainty of the $\Xi(1950)^-$ fit fraction is $+49.9\%$, most of which originates from an alternative fit where its mass and width are floated in the extended model, rather than constrained to the known values [13], while the second largest one, from other

Table 3

Summary of absolute systematic uncertainties for the fit parameters. The units for masses (M_0) and widths (Γ_0) are MeV. The fit fraction in percent is denoted FF.

Source	$P_{cs}(4459)^0$			$\Xi(1690)^-$			$\Xi(1820)^-$			$\Xi(1950)^-$	$\Xi(2030)^-$	NR
	M_0	Γ_0	FF	M_0	Γ_0	FF	M_0	Γ_0	FF	FF	FF	FF
J^P	$+4.7$ -0.3	$+0.0$ -5.7	$+0.1$ -1.3	$+1.2$ -0.1	$+14.0$ -0.9	$+6.7$ -0.3	$+0.8$ -0.2	$+1.4$ -0.5	$+4.2$ -0.3	$+0.2$ -9.4	$+0.0$ -4.1	$+0.9$ -11.2
Model	$+0.7$ -1.1	$+8.0$ -2.0	$+0.7$ -0.5	$+0.5$ -0.4	$+1.8$ -13.5	$+1.9$ -8.9	$+1.0$ -0.6	$+7.8$ -8.2	$+6.9$ -4.1	$+49.9$ -5.4	$+3.8$ -1.6	$+10.3$ -6.4
Λ decay	$+0.0$ -0.7	$+0.0$ -4.7	$+0.0$ -0.3	$+0.0$ -0.4	$+0.2$ -0.0	$+0.0$ -0.8	$+0.0$ -0.5	$+0.0$ -7.2	$+0.0$ -4.1	$+2.4$ -0.0	$+0.0$ -1.3	$+3.9$ -0.0
sWeights	$+0.0$ -0.2	$+0.3$ -0.0	$+0.1$ -0.0	$+0.1$ -0.1	$+3.1$ -0.2	$+1.4$ -0.0	$+0.2$ -0.2	$+2.2$ -1.5	$+1.6$ -0.5	$+0.7$ -1.6	$+0.0$ -0.2	$+0.0$ -2.7
Efficiency	$+0.1$ -0.1	$+0.0$ -0.5	$+0.0$ -0.1	$+0.1$ -0.2	$+2.1$ -1.5	$+0.8$ -1.3	$+0.1$ -0.2	$+1.1$ -0.3	$+0.5$ -0.7	$+2.3$ -1.0	$+0.3$ -0.2	$+1.1$ -0.9
Final	$+4.7$ -1.1	$+8.0$ -5.7	$+0.7$ -1.3	$+1.2$ -0.4	$+14.0$ -13.5	$+6.7$ -8.9	$+1.0$ -0.6	$+7.8$ -8.2	$+6.9$ -4.1	$+49.9$ -9.4	$+3.8$ -4.1	$+10.3$ -11.2

sources considered in the estimation of systematic uncertainty, is +5.9%. Considering this large value, the fit fractions for all components involved in the extended model and their interference fractions are checked. A large interference fraction of −60.3% between $\Xi(1950)^-$ and NR is found in the extended model, and a large width of $\Xi(1950)^-$ of about 350 MeV is found. This could indicate the NR description in the default model is not perfect. Therefore several other NR models discussed before, or the NR contribution replaced by a broad Breit-Wigner function are tested; all of these variations do not change the conclusion on the $P_{cs}(4459)^0$ result.

5. Conclusion

In conclusion, an amplitude analysis of $\Xi_b^- \to J/\psi\Lambda K^-$ decays is performed using approximately 1750 candidates, and a structure in the $J/\psi\Lambda$ mass spectrum around 4459 MeV is seen. This structure can be explained by including a pentaquark candidate with strangeness in the amplitude model. Its significance exceeds 3σ after considering all systematic uncertainties. The mass and width of this new exotic state are measured to be $4458.8 \pm 2.9^{+4.7}_{-1.1}$ MeV and $17.3 \pm 6.5^{+8.0}_{-5.7}$ MeV, respectively. The $P_{cs}(4459)^0$ state has a mass only about 19 MeV below the $\Xi_c^0\bar{D}^{*0}$ threshold and a narrow width. Motivated by this fact, the hypothesis of two resonances contributing to the enhancement is tested. The data cannot confirm or refute the two-peak hypothesis. Furthermore, two Ξ^{*-} states, $\Xi(1690)^-$ and $\Xi(1820)^-$, are observed for the first time in Ξ_b^- decays. Using the full amplitude analysis, their masses and widths are measured to be

$$M(\Xi(1690)^-) = 1692.0 \pm 1.3^{+1.2}_{-0.4}\ \text{MeV},$$
$$\Gamma(\Xi(1690)^-) = 25.9 \pm 9.5^{+14.0}_{-13.5}\ \text{MeV},$$
$$M(\Xi(1820)^-) = 1822.7 \pm 1.5^{+1.0}_{-0.6}\ \text{MeV},$$
$$\Gamma(\Xi(1820)^-) = 36.0 \pm 4.4^{+7.8}_{-8.2}\ \text{MeV}.$$

These results are consistent with the average values reported in the PDG [13] and recent results from the BESIII experiment [14,15]. The mass determinations are much more precise than those listed in the PDG. Due to limited signal yield, the J^P of the $P_{cs}(4459)^0$ and $\Xi(1690)^-$ states are not determined at this stage.

Conflict of interest

The authors declare that they have no conflict of interest.

Acknowledgments

References

[1] Gell-Mann M. A schematic model of baryons and mesons. Phys Lett 1964;8:214.

[2] Zweig G. An SU$_3$ model for strong interaction symmetry and its breaking; Version 1 CERN-TH-401. Geneva: CERN; 1964.

[3] LHCb Collaboration, Aaij R, et al. Observation of $J/\psi p$ resonances consistent with pentaquark states in $\Lambda_b^0 \to J/\psi p K^-$ decays. Phys Rev Lett 2015;115:072001.

[4] LHCb Collaboration, Aaij R, et al. Model-independent evidence for $J/\psi p$ contributions to $\Lambda_b^0 \to J/\psi p K^-$ decays. Phys Rev Lett 2016;117:082002.

[5] LHCb Collaboration, Aaij R, et al. Observation of a narrow pentaquark state, $P_c(4312)^+$, and of two-peak structure of the $P_c(4450)^+$. Phys Rev Lett 2019;122:222001.

[6] Wu J-J, Molina R, Oset E, et al. Prediction of narrow N^* and Λ^* resonances with hidden charm above 4 GeV. Phys Rev Lett 2010;105:232001.

[7] Chen R, He J, Liu X. Possible strange hidden-charm pentaquarks from $\Sigma_c^{(*)}\bar{D}_s^*$ and $\Xi_c^{(\prime,*)}\bar{D}^*$ interactions. Chin Phys C 2017;41:103105.

[8] Santopinto E, Giachino A. Compact pentaquark structures. Phys Rev D 2017;96:014014.

[9] Shen C-W, Wu J-J, Zou B-S. Decay behaviors of possible $\Lambda_{c\bar{c}}$ states in hadronic molecule pictures. Phys Rev D 2019;100:056006.

[10] Xiao C-W, Nieves J, Oset E. Prediction of hidden charm strange molecular baryon states with heavy quark spin symmetry. Phys Lett B 2019;799:135051.

[11] Wang B, Meng L, Zhu S-L. Spectrum of the strange hidden charm molecular pentaquarks in chiral effective field theory. Phys Rev D 2020;101:034018.

[12] Chen H-X, Geng L-S, Liang W-H, et al. Looking for a hidden-charm pentaquark state with strangeness $S = -1$ from Ξ_b^- decay into $J/\psi K^- \Lambda$. Phys Rev C 2016;93:065203.

[13] Particle Data Group, Zyla PA, et al. Review of particle physics. Prog Theor Exp Phys 2020;2020:083C01.

[14] BESIII Collaboration, Ablikim M, et al. Measurements of $\psi(3686) \to K^- \Lambda\bar{\Xi}^+ + c.c.$ and $\psi(3686) \to \gamma K^- \Lambda\bar{\Xi}^+ + c.c.$ Phys Rev D 2015;91:092006.

[15] BESIII Collaboration, Ablikim M, et al. Measurement of the cross section for $e^+e^- \to \Xi^-\bar{\Xi}^+$ and observation of an excited Ξ baryon. Phys Rev Lett 2020;124:032002.

[16] Belle Collaboration, Sumihama M, et al. Observation of the $\Xi(1620)^0$ and evidence for $\Xi(1690)^0$ in $\Xi_c^+ \to \Xi^-\pi^+\pi^+$ decay. Phys Rev Lett 2019;122:072501.

[17] LHCb Collaboration, Aaij R, et al. Observation of the $\Xi_b^- \to J/\psi\Lambda K^-$ decay. Phys Lett B 2017;772:265.

[18] LHCb Collaboration, Alves AA, Jr, et al. The LHCB detector at the LHC. JINST 2008;3:S08005.

[19] LHCb Collaboration, Aaij R, et al. LHCb detector performance. Int J Mod Phys A 2015;30:1530022.

[20] Sjöstrand T, Mrenna S, Skands P. A brief introduction to PYTHIA 8.1. Comput Phys Commun 2008;178:852.

[21] Belyaev I, Brambach T, Brook NH, et al. Handling of the generation of primary events in Gauss, the LHCb simulation framework. J Phys Conf Ser 2011;331:032047.

[22] Lange DJ. The EvtGen particle decay simulation package. Nucl Instrum Methods A 2001;A462:152.

[23] Golonka P, Was Z. PHOTOS Monte Carlo: a precision tool for QED corrections in Z and W decays. Eur Phys J C 2006;45:97.

[24] Davidson N, Przedzinski T, Was Z. PHOTOS interface in C++: technical and physics documentation. Comput Phys Commun 2016;199:86.

[25] Geant4 Collaboration, Allison J, et al. Geant4 developments and applications. IEEE Trans Nucl Sci 2006;53:270.

[26] Geant4 Collaboration, Agostinelli S, et al. Geant4: a simulation toolkit. Nucl Instrum Methods A 2003;506:250.

[27] Clemencic M, Corti G, Easo S, et al. The LHCb simulation application, Gauss: design, evolution and experience. J Phys Conf Ser 2011;331:032023.

[28] Aaij R, Albrecht J, Alessio F, et al. The LHCb trigger and its performance in 2011. JINST 2013;8:P04022.

[29] Breiman L, Friedman JH, Olshen RA, et al. Classification and regression trees. Belmont, California, USA: Wadsworth international group; 1984.

[30] Voss H, Hoecker A, Stelzer J, et al. TMVA – Toolkit for multivariate data analysis with ROOT. PoS ACAT 2007:040.

[31] Hoecker A, Speckmayer P, Stelzer J, et al. TMVA 4 — Toolkit for multivariate data analysis with ROOT. Users Guide. arXiv:0703039, 2007.

[32] Hulsbergen WD. Decay chain fitting with a Kalman filter. Nucl Instrum Methods 2005;A552:566.

[33] Martínez Santos D, Dupertuis F. Mass distributions marginalized over per-event errors. Nucl Instrum Methods A 2014;764:150.

[34] Pivk M, Diberder FRL. sPlot: a statistical tool to unfold data distributions. Nucl Instrum Methods A 2005;A555:356.

[35] Xie Y. sFit: a method for background subtraction in maximum likelihood fit. arXiv:0905.0724, 2009.

[36] JPAC Collaboration, Mikhasenko M, et al. Dalitz-plot decomposition for three-body decays. Phys Rev D 2020;101:034033.

[37] Wang M, Jiang Y, Liu Y, et al. A novel method to test particle ordering and final state alignment in helicity formalism. Chin Phys C 2021;45:063103.

[38] Jacob M, Wick GC. On the general theory of collisions for particles with spin. Ann Phys 1959;7:404.

[39] JPAC Collaboration, Fernández-Ramírez C, et al. Coupled-channel model for $\bar{K}N$ scattering in the resonant region. Phys Rev D 2016;93:034029.

The LHCb experiment

LHCb is one of the four big experiments located on the Large Hadron Collider (LHC) at CERN. The LHCb detector is a single-arm forward spectrometer covering the pseudorapidity range $2 < \eta < 5$, designed for the study of particles containing b or c quarks. The detector includes a silicon-strip vertex detector surrounding the proton-proton interaction region, tracking stations on either side of a dipole magnet, ring-imaging Cherenkov (RICH) detectors, calorimeters and muon chambers. The LHCb Collaboration consists of more than 1400 members from 18 countries in 5 continents, including both physicists and engineers.

LHCb Collaboration

R. Aaij[32], C. Abellán Beteta[50], T. Ackernley[60], B. Adeva[46], M. Adinolfi[54], H. Afsharnia[9], C.A. Aidala[85], S. Aiola[26], Z. Ajaltouni[9], S. Akar[65], J. Albrecht[15], F. Alessio[48], M. Alexander[59], A. Alfonso Albero[45], Z. Aliouche[62], G. Alkhazov[38], P. Alvarez Cartelle[55], S. Amato[2], Y. Amhis[11], L. An[48], L. Anderlini[22], A. Andreianov[38], M. Andreotti[21], F. Archilli[17], A. Artamonov[44], M. Artuso[68], K. Arzymatov[42], E. Aslanides[10], M. Atzeni[50], B. Audurier[12], S. Bachmann[17], M. Bachmayer[49], J.J. Back[56], S. Baker[61], P. Baladron Rodriguez[46], V. Balagura[12], W. Baldini[21,48], J. Baptista Leite[1], R.J. Barlow[62], S. Barsuk[11], W. Barter[61], M. Bartolini[24,h], F. Baryshnikov[81], J.M. Basels[14], G. Bassi[29], B. Batsukh[68], A. Battig[15], A. Bay[49], M. Becker[15], F. Bedeschi[29], I. Bediaga[1], A. Beiter[68], V. Belavin[42], S. Belin[27], V. Bellee[49], K. Belous[44], I. Belov[40], I. Belyaev[39], G. Bencivenni[23], E. Ben-Haim[13], A. Berezhnoy[40], R. Bernet[50], D. Berninghoff[17], H.C. Bernstein[68], C. Bertella[48], E. Bertholet[13], A. Bertolin[28], C. Betancourt[50], F. Betti[20,d], Ia. Bezshyiko[50], S. Bhasin[54], J. Bhom[34], L. Bian[73], M.S. Bieker[15], S. Bifani[53], P. Billoir[13], M. Birch[61], F.C.R. Bishop[55], A. Bizzeti[22,r], M. Bjørn[63], M.P. Blago[48], T. Blake[56], F. Blanc[49], S. Blusk[68], D. Bobulska[59], J.A. Boelhauve[15], O. Boente Garcia[46], T. Boettcher[64], A. Boldyrev[82], A. Bondar[43], N. Bondar[38,48], S. Borghi[62], M. Borisyak[42], M. Borsato[17], J.T. Borsuk[34], S.A. Bouchiba[49], T.J.V. Bowcock[60], A. Boyer[48], C. Bozzi[21], M. J. Bradley[61], S. Braun[66], A. Brea Rodriguez[46], M. Brodski[48], J. Brodzicka[34], A. Brossa Gonzalo[56], D. Brundu[27], A. Buonaura[50], C. Burr[48], A. Bursche[27], A. Butkevich[41], J.S. Butter[32], J. Buytaert[48], W. Byczynski[48], S. Cadeddu[27], H. Cai[73], R. Calabrese[21,f], L. Calefice[15,13], L. Calero Diaz[23], S. Cali[23], R. Calladine[53], M. Calvi[25,i], M. Calvo Gomez[84], P. Camargo Magalhaes[54], A. Camboni[45], P. Campana[23], A.F. Campoverde Quezada[5], S. Capelli[25,i], L. Capriotti[20,d], A. Carbone[20,d], G. Carboni[30], R. Cardinale[24,h], A. Cardini[27], I. Carli[6], P. Carniti[25,i], L. Carus[14], K. Carvalho Akiba[32], A. Casais Vidal[46], G. Casse[60], M. Cattaneo[48], G. Cavallero[48], S. Celani[49], J. Cerasoli[10], A.J. Chadwick[60], M.G. Chapman[54], M. Charles[13], Ph. Charpentier[48], G. Chatzikonstantinidis[53], C.A. Chavez Barajas[60], M. Chefdeville[8], C. Chen[3], S. Chen[27], A. Chernov[34], S.-G. Chitic[48], V. Chobanova[46], S. Cholak[49], M. Chrzaszcz[34], A. Chubykin[38], V. Chulikov[38], P. Ciambrone[23], M.F. Cicala[56], X. Cid Vidal[46], G. Ciezarek[48], P.E.L. Clarke[58], M. Clemencic[48], H.V. Cliff[55], J. Closier[48], J.L. Cobbledick[62], V. Coco[48], J.A.B. Coelho[11], J. Cogan[10], E. Cogneras[9], L. Cojocariu[37], P. Collins[48], T. Colombo[48], L. Congedo[19,c], A. Contu[27], N. Cooke[53], G. Coombs[59], G. Corti[48], C.M. Costa Sobral[56], B. Couturier[48], D.C. Craik[64], J. Crkovská[67], M. Cruz Torres[1], R. Currie[58], C.L. Da Silva[67], E. Dall'Occo[15], J. Dalseno[46], C. D'Ambrosio[48], A. Danilina[39], P. d'Argent[48], A. Davis[62], O. De Aguiar Francisco[62], K. De Bruyn[78], S. De Capua[62], M. De Cian[49], J.M. De Miranda[1], L. De Paula[2], M. De Serio[19,c], D. De Simone[50], P. De Simone[23], J.A. de Vries[79], C.T. Dean[67], W. Dean[85], D. Decamp[8], L. Del Buono[13], B. Delaney[55], H.-P. Dembinski[15], A. Dendek[35], V. Denysenko[50], D. Derkach[82], O. Deschamps[9], F. Desse[11], F. Dettori[27,e], B. Dey[73], P. Di Nezza[23], S. Didenko[81], L. Dieste Maronas[46], H. Dijkstra[48], V. Dobishuk[52], A.M. Donohoe[18], F. Dordei[27], A.C. dos Reis[1], L. Douglas[59], A. Dovbnya[51], A.G. Downes[8], K. Dreimanis[60], M.W. Dudek[34], L. Dufour[48], V. Duk[77], P. Durante[48], J.M. Durham[67], D. Dutta[62], M. Dziewiecki[17], A. Dziurda[34], A. Dzyuba[38], S. Easo[57], U. Egede[69], V. Egorychev[39], S. Eidelman[43,u], S. Eisenhardt[58], S. Ek-In[49], L. Eklund[59], S. Ely[68], A. Ene[37], E. Epple[67], S. Escher[14], J. Eschle[50], S. Esen[32], T. Evans[48], A. Falabella[20], J. Fan[3], Y. Fan[5], B. Fang[73], N. Farley[53], S. Farry[60], D. Fazzini[25, i], P. Fedin[39], M. Féo[48], P. Fernandez Declara[48], A. Fernandez Prieto[46], J.M. Fernandez-tenllado Arribas[45], F. Ferrari[20,d], L. Ferreira Lopes[49], F. Ferreira Rodrigues[2], S. Ferreres Sole[32], M. Ferrillo[50], M. Ferro-Luzzi[48], S. Filippov[41], R.A. Fini[19], M. Fiorini[21,f], M. Firlej[35], K.M. Fischer[63], C. Fitzpatrick[62], T. Fiutowski[35], F. Fleuret[12], M. Fontana[13], F. Fontanelli[24,h], R. Forty[48], V. Franco Lima[60], M. Franco Sevilla[66], M. Frank[48], E. Franzoso[21], G. Frau[17], C. Frei[48], D.A. Friday[59], J. Fu[26], Q. Fuehring[15], W. Funk[48], E. Gabriel[32], T. Gaintseva[42], A. Gallas Torreira[46], D. Galli[20,d], S. Gambetta[58,48], Y. Gan[3], M. Gandelman[2], P. Gandini[26], Y. Gao[4], M. Garau[27], L. M. Garcia Martin[56], P. Garcia Moreno[45], J. García Pardiñas[25], B. Garcia Plana[46], F.A. Garcia Rosales[12], L. Garrido[45], C. Gaspar[48], R.E. Geertsema[32], D. Gerick[17], L.L. Gerken[15], E. Gersabeck[62], M. Gersabeck[62], T. Gershon[56], D. Gerstel[10], Ph. Ghez[8], V. Gibson[55], M. Giovannetti[23,j], A. Gioventù[46], P. Gironella Gironell[45], L. Giubega[37], C. Giugliano[21,48,f], K. Gizdov[58], E.L. Gkougkousis[48], V.V. Gligorov[13], C. Göbel[70], E. Golo-

bardes[84], D. Golubkov[39], A. Golutvin[61,81], A. Gomes[1,a], S. Gomez Fernandez[45], F. Goncalves Abrantes[70], M. Goncerz[34], G. Gong[3], P. Gorbounov[39], I.V. Gorelov[40], C. Gotti[25], E. Govorkova[48], J.P. Grabowski[17], R. Graciani Diaz[45], T. Grammatico[13], L.A. Granado Cardoso[48], E. Graugés[45], E. Graverini[49], G. Graziani[22], A. Grecu[37], L.M. Greeven[32], P. Griffith[21], L. Grillo[62], S. Gromov[81], B.R. Gruberg Cazon[63], C. Gu[3], M. Guarise[21], P. A. Günther[17], E. Gushchin[41], A. Guth[14], Y. Guz[44,48], T. Gys[48], T. Hadavizadeh[69], G. Haefeli[49], C. Haen[48], J. Haimberger[48], T. Halewood-leagas[60], P.M. Hamilton[66], Q. Han[7], X. Han[17], T.H. Hancock[63], S. Hansmann-Menzemer[17], N. Harnew[63], T. Harrison[60], C. Hasse[48], M. Hatch[48], J. He[5], M. Hecker[61], K. Heijhoff[32], K. Heinicke[15], A.M. Hennequin[48], K. Hennessy[60], L. Henry[26,47], J. Heuel[14], A. Hicheur[2], D. Hill[49], M. Hilton[62], S.E. Hollitt[15], J. Hu[17], J. Hu[72], W. Hu[7], W. Huang[5], X. Huang[73], W. Hulsbergen[32], R.J. Hunter[56], M. Hushchyn[82], D. Hutchcroft[60], D. Hynds[32], P. Ibis[15], M. Idzik[35], D. Ilin[38], P. Ilten[65], A. Inglessi[38], A. Ishteev[81], K. Ivshin[38], R. Jacobsson[48], S. Jakobsen[48], E. Jans[32], B.K. Jashal[47], A. Jawahery[66], V. Jevtic[15], M. Jezabek[34], F. Jiang[3], M. John[63], D. Johnson[48], C.R. Jones[55], T.P. Jones[56], B. Jost[48], N. Jurik[48], S. Kandybei[51], Y. Kang[3], M. Karacson[48], M. Karpov[82], N. Kazeev[82], F. Keizer[55,48], M. Kenzie[56], T. Ketel[33], B. Khanji[15], A. Kharisova[83], S. Kholodenko[44], K.E. Kim[68], T. Kirn[14], V.S. Kirsebom[49], O. Kitouni[64], S. Klaver[32], K. Klimaszewski[36], S. Koliiev[52], A. Kondybayeva[81], A. Konoplyannikov[39], P. Kopciewicz[35], R. Kopecna[17], P. Koppenburg[32], M. Korolev[40], I. Kostiuk[32,52], O. Kot[52], S. Kotriakhova[38,31], P. Kravchenko[38], L. Kravchuk[41], R.D. Krawczyk[48], M. Kreps[56], F. Kress[61], S. Kretzschmar[14], P. Krokovny[43,u], W. Krupa[35], W. Krzemien[36], W. Kucewicz[34,k], M. Kucharczyk[34], V. Kudryavtsev[43,u], H.S. Kuindersma[32], G.J. Kunde[67], T. Kvaratskheliya[39], D. Lacarrere[48], G. Lafferty[62], A. Lai[27], A. Lampis[27], D. Lancierini[50], J.J. Lane[62], R. Lane[54], G. Lanfranchi[23], C. Langenbruch[14], J. Langer[15], O. Lantwin[50,81], T. Latham[56], F. Lazzari[29,s], R. Le Gac[10], S.H. Lee[85], R. Lefèvre[9], A. Leflat[40], S. Legotin[81], O. Leroy[10], T. Lesiak[34], B. Leverington[17], H. Li[72], L. Li[63], P. Li[17], Y. Li[6], Y. Li[6], Z. Li[68], X. Liang[68], T. Lin[61], R. Lindner[48], V. Lisovskyi[15], R. Litvinov[27], G. Liu[72], H. Liu[5], S. Liu[6], X. Liu[3], A. Loi[27], J. Lomba Castro[46], I. Longstaff[59], J.H. Lopes[2], G. Loustau[50], G.H. Lovell[55], Y. Lu[6], D. Lucchesi[28,l], S. Luchuk[41], M. Lucio Martinez[32], V. Lukashenko[32], Y. Luo[3], A. Lupato[62], E. Luppi[21,f], O. Lupton[56], A. Lusiani[29,q], X. Lyu[5], L. Ma[6], R. Ma[5], S. Maccolini[20,d], F. Machefert[11], F. Maciuc[37], V. Macko[49], P. Mackowiak[15], S. Maddrell-Mander[54], O. Madejczyk[35], L.R. Madhan Mohan[54], O. Maev[38], A. Maevskiy[82], D. Maisuzenko[38], M.W. Majewski[35], J.J. Malczewski[34], S. Malde[63], B. Malecki[48], A. Malinin[80], T. Maltsev[43,u], H. Malygina[17], G. Manca[27,e], G. Mancinelli[10], R. Manera Escalero[45], D. Manuzzi[20,d], D. Marangotto[26,n], J. Maratas[9,t], J.F. Marchand[8], U. Marconi[20], S. Mariani[22,48,g], C. Marin Benito[11], M. Marinangeli[49], P. Marino[49], J. Marks[17], P.J. Marshall[60], G. Martellotti[31], L. Martinazzoli[48,i], M. Martinelli[25,i], D. Martinez Santos[46], F. Martinez Vidal[47], A. Massafferri[1], M. Materok[14], R. Matev[48], A. Mathad[50], Z. Mathe[48], V. Matiunin[39], C. Matteuzzi[25], K.R. Mattioli[85], A. Mauri[32], E. Maurice[12], J. Mauricio[45], M. Mazurek[36], M. McCann[61], L. Mcconnell[18], T.H. Mcgrath[62], A. McNab[62], R. McNulty[18], J.V. Mead[60], B. Meadows[65], C. Meaux[10], G. Meier[15], N. Meinert[76], D. Melnychuk[36], S. Meloni[25,i], M. Merk[32,79], A. Merli[26], L. Meyer Garcia[2], M. Mikhasenko[48], D.A. Milanes[74], E. Millard[56], M. Milovanovic[48], M.-N. Minard[8], L. Minzoni[21,f], S.E. Mitchell[58], B. Mitreska[62], D.S. Mitzel[48], A. Mödden[15], R.A. Mohammed[63], R.D. Moise[61], T. Mombächer[15], I.A. Monroy[74], S. Monteil[9], M. Morandin[28], G. Morello[23], M.J. Morello[29,q], J. Moron[35], A.B. Morris[75], A.G. Morris[56], R. Mountain[68], H. Mu[3], F. Muheim[58], M. Mukherjee[7], M. Mulder[48], D. Müller[48], K. Müller[50], C. H. Murphy[63], D. Murray[62], P. Muzzetto[27,48], P. Naik[54], T. Nakada[49], R. Nandakumar[57], T. Nanut[49], I. Nasteva[2], M. Needham[58], I. Neri[21,f], N. Neri[26,n], S. Neubert[75], N. Neufeld[48], R. Newcombe[61], T.D. Nguyen[49], C. Nguyen-Mau[49], E.M. Niel[11], S. Nieswand[14], N. Nikitin[40], N.S. Nolte[48], C. Nunez[85], A. Oblakowska-Mucha[35], V. Obraztsov[44], D.P. O'Hanlon[54], R. Oldeman[27,e], M.E. Olivares[68], C.J.G. Onderwater[78], A. Ossowska[34], J. M. Otalora Goicochea[2], T. Ovsiannikova[39], P. Owen[50], A. Oyanguren[47], B. Pagare[56], P.R. Pais[48], T. Pajero[29,48,q], A. Palano[19], M. Palutan[23], Y. Pan[62], G. Panshin[83], A. Papanestis[57], M. Pappagallo[19,c], L.L. Pappalardo[21,f], C. Pappenheimer[65], W. Parker[66], C. Parkes[62], C.J. Parkinson[46], B. Passalacqua[21], G. Passaleva[22], A. Pastore[19], M. Patel[61], C. Patrignani[20,d], C.J. Pawley[79], A. Pearce[48], A. Pellegrino[32], M. Pepe Altarelli[48], S. Perazzini[20], D. Pereima[39], P. Perret[9], K. Petridis[54], A. Petrolini[24,h], A. Petrov[80], S. Petrucci[58], M. Petruzzo[26], T.T.H. Pham[68], A. Philippov[42], L. Pica[29], M. Piccini[77], B. Pietrzyk[8], G. Pietrzyk[49], M. Pili[63], D. Pinci[31], F. Pisani[48], A. Piucci[17], Resmi P.K[10], V. Placinta[37], J. Plews[53], M. Plo Casasus[46], F. Polci[13], M. Poli Lener[23], M. Poliakova[68], A. Poluektov[10], N. Polukhina[81,b], I. Polyakov[68], E. Polycarpo[2], G.J. Pomery[54], S. Ponce[48], D. Popov[5,48], S. Popov[42], S. Poslavskii[44], K. Prasanth[34], L. Promberger[48], C. Prouve[46], V. Pugatch[52], H. Pullen[63], G. Punzi[29,m], W. Qian[5], J. Qin[5], R. Quagliani[13], B. Quintana[8], N.V. Raab[18], R.I. Rabadan Trejo[10], B. Rachwal[35], J.H. Rademacker[54], M. Rama[29], M. Ramos Pernas[56], M.S. Rangel[2], F. Ratnikov[42,82], G. Raven[33], M. Reboud[8], F. Redi[49], F. Reiss[13], C. Remon Alepuz[47], Z. Ren[3], V. Renaudin[63], R. Ribatti[29], S. Ricciardi[57], K. Rinnert[60], P. Robbe[11], A. Robert[13], G. Robertson[58], A.B. Rodrigues[49], E. Rodrigues[60], J.A. Rodriguez Lopez[74], A. Rollings[63], P. Roloff[48], V. Romanovskiy[44], M. Romero Lamas[46], A. Romero Vidal[46], J.D. Roth[85], M. Rotondo[23], M.S. Rudolph[68], T. Ruf[48], J. Ruiz Vidal[47], A. Ryzhikov[82], J. Ryzka[35], J.J. Saborido Silva[46], N. Sagidova[38], N. Sahoo[56], B. Saitta[27,e], D. Sanchez Gonzalo[45], C. Sanchez Gras[32], R. Santacesaria[31], C. Santamarina Rios[46], M. Santimaria[23], E. Santovetti[30,j], D. Saranin[81], G. Sarpis[59], M. Sarpis[75], A. Sarti[31], C. Satriano[31,p], A. Satta[30], M. Saur[15], D. Savrina[39,40], H. Sazak[9], L.G. Scantlebury Smead[63], S. Schael[14], M. Schellenberg[15], M. Schiller[59], H. Schindler[48], M. Schmelling[16], B. Schmidt[48], O. Schneider[49], A. Schopper[48], M. Schubiger[32], S. Schulte[49], M.H. Schune[11], R. Schwemmer[48], B. Sciascia[23], A. Sciubba[31], S. Sellam[46], A. Semennikov[39], M. Senghi Soares[33], A. Sergi[53,48], N. Serra[50], L. Sestini[28], A. Seuthe[15], P. Seyfert[48], D.M. Shangase[85], M. Shapkin[44], I. Shchemerov[81], L. Shchutska[49], T. Shears[60], L. Shekhtman[43,u], Z. Shen[4], V. Shevchenko[80], E.B. Shields[25,i], E. Shmanin[81], J.D. Shupperd[68], B.G. Siddi[21], R. Silva Coutinho[50], G. Simi[28], S. Simone[19,c], I. Skiba[21,f], N. Skidmore[62], T. Skwarnicki[68], M.W. Slater[53], J.C. Smallwood[63], J.G. Smeaton[55], A. Smetkina[39], E. Smith[14], M. Smith[61], A. Snoch[32], M. Soares[20], L. Soares Lavra[9], M.D. Sokoloff[65], F.J.P. Soler[59], A. Solovev[38], I. Solovyev[38], F.L. Souza De Almeida[2], B. Souza De Paula[2], B. Spaan[15], E. Spadaro Norella[26,n], P. Spradlin[59], F. Stagni[48], M. Stahl[65], S. Stahl[48], P. Stefko[49], O. Steinkamp[50,81], S. Stemmle[17], O. Stenyakin[44], H. Stevens[15], S. Stone[68], M.E. Stramaglia[49], M. Straticiuc[37], D. Strekalina[81], S. Strokov[83], F. Suljik[63], J. Sun[27], L. Sun[73], Y. Sun[66], P. Svihra[62], P.N. Swallow[53], K. Swientek[35], A. Szabelski[36], T. Szumlak[35], M. Szymanski[48], S. Taneja[62], F. Teubert[48], E. Thomas[48], K.A. Thomson[60], M.J. Tilley[61], V. Tisserand[9], S. T'Jampens[8], M. Tobin[6], S. Tolk[48], L. Tomassetti[21,f], D. Torres Machado[1], D.Y. Tou[13], M. Traill[59], M.T. Tran[49], E. Trifonova[81], C. Trippl[49], G. Tuci[29,m], A. Tully[49], N. Tuning[32], A. Ukleja[36], D.J. Unverzagt[17], E. Ursov[81], A. Usachov[32], A. Ustyuzhanin[42,82], U. Uwer[17], A. Vagner[83], V. Vagnoni[20], A. Valassi[48], G. Valenti[20], N. Valls Canudas[45], M. van Beuzekom[32], M. Van Dijk[49], E. van Herwijnen[81], C.B. Van Hulse[18], M. van Veghel[78], R. Vazquez Gomez[46], P. Vazquez Regueiro[46], C. Vázquez Sierra[48], S. Vecchi[21], J.J. Velthuis[54], M. Veltri[22,o], A. Venkateswaran[68], M. Veronesi[32], M. Vesterinen[56], D. Vieira[65], M. Vieites Diaz[49], H. Viemann[76], X. Vilasis-Cardona[84], E. Vilella Figueras[60], P. Vincent[13], G. Vitali[29], A. Vollhardt[50], D. Vom Bruch[13], A. Vorobyev[38], V. Vorobyev[43,u], N. Voropaev[38], R. Waldi[76], J. Walsh[29], C. Wang[17], J. Wang[3], J. Wang[73], J. Wang[4], J. Wang[6], M. Wang[3], R. Wang[54], Y. Wang[7], Z. Wang[50], H.M. Wark[60], N.K. Watson[53], S.G. Weber[13], D. Websdale[61], C. Weisser[64], B.D. C. Westhenry[54], D.J. White[62], M. Whitehead[54], D. Wiedner[15], G. Wilkinson[63], M. Wilkinson[68], I. Williams[55], M. Williams[64,69], M.R.J. Williams[58], F.F. Wilson[57], W. Wislicki[36], M. Witek[34], L. Witola[17], G. Wormser[11], S.A. Wotton[55], H. Wu[68], K. Wyllie[48], Z. Xiang[5], D. Xiao[7], Y. Xie[7], A. Xu[4], J. Xu[5], L. Xu[3], M. Xu[7], Q. Xu[5], Z. Xu[5], Z. Xu[4], D. Yang[7], S. Yang[5], Y. Yang[5], Z. Yang[3], Z. Yang[66], Y. Yao[68], L.E. Yeomans[60], H. Yin[7], J. Yu[71], X. Yuan[68], O. Yushchenko[44], E. Zaffaroni[49], K.A. Zarebski[53], M. Zavertyaev[16,b], M. Zdybal[34], O. Zenaiev[48], M. Zeng[3], D. Zhang[7], L. Zhang[3], S. Zhang[4], Y. Zhang[4], Y. Zhang[63], A. Zhelezov[17], Y. Zheng[5], X. Zhou[5], Y. Zhou[5], X. Zhu[3], V. Zhukov[14,40], J.B. Zonneveld[58], S. Zucchelli[20,d], D. Zuliani[28], G. Zunica[62]

[1] Centro Brasileiro de Pesquisas Físicas (CBPF), Rio de Janeiro, Brazil
[2] Universidade Federal do Rio de Janeiro (UFRJ), Rio de Janeiro, Brazil
[3] Center for High Energy Physics, Tsinghua University, Beijing, China
[4] School of Physics State Key Laboratory of Nuclear Physics and Technology, Peking University, Beijing, China
[5] University of Chinese Academy of Sciences, Beijing, China
[6] Institute Of High Energy Physics (IHEP), Beijing, China
[7] Institute of Particle Physics, Central China Normal University, Wuhan, Hubei, China
[8] Univ. Grenoble Alpes, Univ. Savoie Mont Blanc, CNRS, IN2P3-LAPP, Annecy, France
[9] Université Clermont Auvergne, CNRS/IN2P3, LPC, Clermont-Ferrand, France
[10] Aix Marseille Univ, CNRS/IN2P3, CPPM, Marseille, France
[11] Université Paris-Saclay, CNRS/IN2P3, IJCLab, Orsay, France
[12] Laboratoire Leprince-ringuet (llr), Palaiseau, France
[13] LPNHE, Sorbonne Université, Paris Diderot Sorbonne Paris Cité, CNRS/IN2P3, Paris, France
[14] I. Physikalisches Institut, RWTH Aachen University, Aachen, Germany
[15] Fakultät Physik, Technische Universität Dortmund, Dortmund, Germany
[16] Max-Planck-Institut für Kernphysik (MPIK), Heidelberg, Germany
[17] Physikalisches Institut, Ruprecht-Karls-Universität Heidelberg, Heidelberg, Germany
[18] School of Physics, University College Dublin, Dublin, Ireland
[19] INFN Sezione di Bari, Bari, Italy
[20] INFN Sezione di Bologna, Bologna, Italy
[21] INFN Sezione di Ferrara, Ferrara, Italy
[22] INFN Sezione di Firenze, Firenze, Italy
[23] INFN Laboratori Nazionali di Frascati, Frascati, Italy
[24] INFN Sezione di Genova, Genova, Italy
[25] INFN Sezione di Milano-Bicocca, Milano, Italy
[26] INFN Sezione di Milano, Milano, Italy
[27] INFN Sezione di Cagliari, Monserrato, Italy
[28] Universita degli Studi di Padova, Universita e INFN, Padova, Padova, Italy
[29] INFN Sezione di Pisa, Pisa, Italy
[30] INFN Sezione di Roma Tor Vergata, Roma, Italy
[31] INFN Sezione di Roma La Sapienza, Roma, Italy
[32] Nikhef National Institute for Subatomic Physics, Amsterdam, Netherlands
[33] Nikhef National Institute for Subatomic Physics and VU University Amsterdam, Amsterdam, Netherlands
[34] Henryk Niewodniczanski Institute of Nuclear Physics Polish Academy of Sciences, Kraków, Poland
[35] AGH - University of Science and Technology, Faculty of Physics and Applied Computer Science, Kraków, Poland
[36] National Center for Nuclear Research (NCBJ), Warsaw, Poland
[37] Horia Hulubei National Institute of Physics and Nuclear Engineering, Bucharest-Magurele, Romania
[38] Petersburg Nuclear Physics Institute NRC Kurchatov Institute (PNPI NRC KI), Gatchina, Russia
[39] Institute of Theoretical and Experimental Physics NRC Kurchatov Institute (ITEP NRC KI), Moscow, Russia
[40] Institute of Nuclear Physics, Moscow State University (SINP MSU), Moscow, Russia
[41] Institute for Nuclear Research of the Russian Academy of Sciences (INR RAS), Moscow, Russia
[42] Yandex School of Data Analysis, Moscow, Russia
[43] Budker Institute of Nuclear Physics (SB RAS), Novosibirsk, Russia
[44] Institute for High Energy Physics NRC Kurchatov Institute (IHEP NRC KI), Protvino, Russia, Protvino, Russia
[45] ICCUB, Universitat de Barcelona, Barcelona, Spain
[46] Instituto Galego de Física de Altas Enerxías (IGFAE), Universidade de Santiago de Compostela, Santiago de Compostela, Spain
[47] Instituto de Fisica Corpuscular, Centro Mixto Universidad de Valencia - CSIC, Valencia, Spain
[48] European Organization for Nuclear Research (CERN), Geneva, Switzerland
[49] Institute of Physics, Ecole Polytechnique Fédérale de Lausanne (EPFL), Lausanne, Switzerland
[50] Physik-Institut, Universität Zürich, Zürich, Switzerland
[51] NSC Kharkiv Institute of Physics and Technology (NSC KIPT), Kharkiv, Ukraine
[52] Institute for Nuclear Research of the National Academy of Sciences (KINR), Kyiv, Ukraine
[53] University of Birmingham, Birmingham, United Kingdom
[54] H.H. Wills Physics Laboratory, University of Bristol, Bristol, United Kingdom
[55] Cavendish Laboratory, University of Cambridge, Cambridge, United Kingdom
[56] Department of Physics, University of Warwick, Coventry, United Kingdom
[57] STFC Rutherford Appleton Laboratory, Didcot, United Kingdom
[58] School of Physics and Astronomy, University of Edinburgh, Edinburgh, United Kingdom
[59] School of Physics and Astronomy, University of Glasgow, Glasgow, United Kingdom
[60] Oliver Lodge Laboratory, University of Liverpool, Liverpool, United Kingdom
[61] Imperial College London, London, United Kingdom
[62] Department of Physics and Astronomy, University of Manchester, Manchester, United Kingdom
[63] Department of Physics, University of Oxford, Oxford, United Kingdom
[64] Massachusetts Institute of Technology, Cambridge, MA, United States
[65] University of Cincinnati, Cincinnati, OH, United States
[66] University of Maryland, College Park, MD, United States

[67] Los Alamos National Laboratory (LANL), Los Alamos, United States

[68] Syracuse University, Syracuse, NY, United States

[69] School of Physics and Astronomy, Monash University, Melbourne, Australia, associated to [56]

[70] Pontifícia Universidade Católica do Rio de Janeiro (PUC-Rio), Rio de Janeiro, Brazil, associated to [2]

[71] Physics and Micro Electronic College, Hunan University, Changsha City, China, associated to [7]

[72] Guangdong Provencial Key Laboratory of Nuclear Science, Institute of Quantum Matter, South China Normal University, Guangzhou, China, associated to [3]

[73] School of Physics and Technology, Wuhan University, Wuhan, China, associated to [3]

[74] Departamento de Fisica , Universidad Nacional de Colombia, Bogota, Colombia, associated to [13]

[75] Universität Bonn - Helmholtz-Institut für Strahlen und Kernphysik, Bonn, Germany, associated to [17]

[76] Institut für Physik, Universität Rostock, Rostock, Germany, associated to [17]

[77] INFN Sezione di Perugia, Perugia, Italy, associated to [21]

[78] Van Swinderen Institute, University of Groningen, Groningen, Netherlands, associated to [32]

[79] Universiteit Maastricht, Maastricht, Netherlands, associated to [32]

[80] National Research Centre Kurchatov Institute, Moscow, Russia, associated to [39]

[81] National University of Science and Technology "MISIS", Moscow, Russia, associated to [39]

[82] National Research University Higher School of Economics, Moscow, Russia, associated to [42]

[83] National Research Tomsk Polytechnic University, Tomsk, Russia, associated to [39]

[84] DS4DS, La Salle, Universitat Ramon Llull, Barcelona, Spain, associated to [45]

[85] University of Michigan, Ann Arbor, United States, associated to [68]

[a] Universidade Federal do Triângulo Mineiro (UFTM), Uberaba-MG, Brazil

[b] P.N. Lebedev Physical Institute, Russian Academy of Science (LPI RAS), Moscow, Russia

[c] Università di Bari, Bari, Italy

[d] Università di Bologna, Bologna, Italy

[e] Università di Cagliari, Cagliari, Italy

[f] Università di Ferrara, Ferrara, Italy

[g] Università di Firenze, Firenze, Italy

[h] Università di Genova, Genova, Italy

[i] Università di Milano Bicocca, Milano, Italy

[j] Università di Roma Tor Vergata, Roma, Italy

[k] AGH - University of Science and Technology, Faculty of Computer Science, Electronics and Telecommunications, Kraków, Poland

[l] Università di Padova, Padova, Italy

[m] Università di Pisa, Pisa, Italy

[n] Università degli Studi di Milano, Milano, Italy

[o] Università di Urbino, Urbino, Italy

[p] Università della Basilicata, Potenza, Italy

[q] Scuola Normale Superiore, Pisa, Italy

[r] Università di Modena e Reggio Emilia, Modena, Italy

[s] Università di Siena, Siena, Italy

[t] MSU - Iligan Institute of Technology (MSU-IIT), Iligan, Philippines

[u] Novosibirsk State University, Novosibirsk, Russia